UNIVERSITY OF PENNSYLVANIA

ELECTRICAL ENGINEERING DEPARTMENT

3RD Quarterly Report
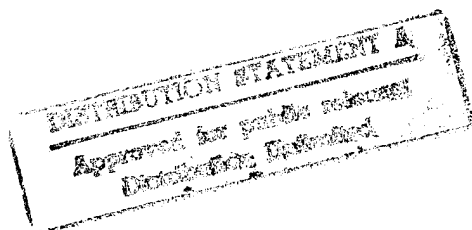
COGNITIVE NETWORKS FOR ATR:
THE ROLES OF BIFURCATION AND CHAOS

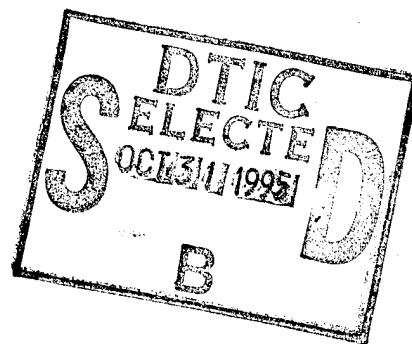Period Covered: 01/01/95 - 04/01/95

Submitted to:

OFFICE OF NAVAL RESEARCH

Principal Investigator

Nabil H. Farhat

April 1, 1995

During the period of this report, we completed construction of what we believe to be the first neural network of biology-like pulsating neuron. The network consists of N=32 PUTONs (programmable unijunction transistor neurons). The coupling between neurons was realized by way of a JPL programmable synaptic weight chip. Methods for monitoring the collective firing activity and characterizing the spiking behavior of neurons in the network were also developed. A simplified circuit diagram of the network, with only one PUTON shown, is given in Fig. 1. The mode of coupling between neuron and mutual control of firing activity in this first embodiment is via modulation of the grid voltage of the PUTON by the net input from its presynaptic neurons. Other modes of coupling, e.g. by modulating the extinction voltage will be studied in the future.

To date, we find that when the connection weights matrix is selected randomly, the network cannot reach phase-lock. However any structuring in the connectivity matrix results usually in phase-locking manifested by ordered firing of the neurons. The network is capable therefore of self-organization which makes it potentially capable of carrying out optimization and learning tasks. We have also verified that when phase-lock is established, the net synaptic input to each neuron is periodic (see Fig. 2). This justifies our earlier use of periodic (cosinusoidal) signals to characterize the behavior of a single isolated PUTON by bifurcation diagrams, that illustrate the functional complexity of these processing units.

One important aspect of exploring the dynamics of the pulsating network is that it demonstrates potential for solving temporal optimization problems whose solutions involve a temporal ordering of events; a good example is the N-city Traveling Salesman Problem (TSP-N). Spiking networks in this regard have an advantage over embedding and solving TSP-N in networks of sigmoidal neurons in that only N spiking neurons are needed instead of the usual N^2 sigmoidal neuron. This can be significant advantage when N is large. Furthermore, the speed advantage of solving the TSP-N with analog hardware over numerical (digital) solutions is preserved in spiking network. This speed advantage becomes significant as N is increased, because while solution time in digital hardware grows exponentially with N, the time needed to reach phase-lock in our pulsating network does not change significantly with N (N was changed from N=5 to its maximum value in our network $N_{max} = 32$).

Several techniques for inducing meaningful phase-lock states in our network were studied. One simple method of setting initial conditions for the network that we used, is to temporarily reduce the supply voltage of the PUTONs to a low value, such that none of the neurons can fire, and then gradually increase the supply voltage back to its original value. In many cases, the network will reach another steady-state (phase-lock state), which will sometimes correspond to a better solution. Another, is a method for annealing the network by temporarily removing one of

1
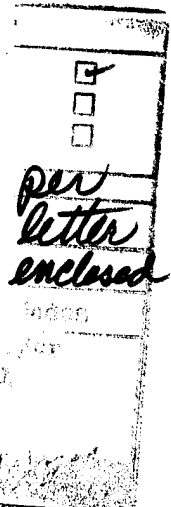
the neurons from the network, and then re-inserting it. This is accomplished by temporarily setting the weights between a specified neuron and each of the remaining neurons to zero, and then returning them to their original values.

A way of allowing the system to develop in a specific order is to include only two neurons in the network in the beginning, and then gradually include one by one other neurons into the network. This procedure can be realized by setting the weights to zero for those neurons not included in the network, and then gradually changing the relevant weights to the desired values. The order in which the neurons are added can however influence the steady-state solutions of the system.

In our experiments on the network, we focused on the phase-locking phenomenon of the network as a possible mechanism for solving optimization problems. There are, however, other dynamics of the network that can be exploited. From the experiments performed on single neurons, we know that our neuron models can exhibit chaotic dynamics. Therefore, there are other possible applications of such behavior to be explored. Further work in studying the network of pulsed neurons is to build networks that implement other mechanisms of coupling among the neurons. It can be expected that such networks will exhibit more complicated dynamics than those exhibited so far by our current network.

One goal of our work with the spiking network is to gain insight into how the order of firing of neurons can be controlled by the weights matrix and initial conditions. This facet of the work is important because it is related to the more challenging task of finding a rule or algorithm for learning in pulsating neural networks. A learning rule for pulsating neural network would have far reaching implications because it implies ability to learn, recognize, or generate spatio-temporal patterns more naturally and directly than in the limited methods developed for sigmoidal networks.

During the period of this report, two reports of our research under this grant were published:

1. Z. Wen, A. Baek, and N.H. Farhat, "Optoelectronic neural dendritic tree processing with electron-trapping materials", Optics Letters, vol. 20, pp. 614-616, March, 1995.

1. J.R. Tower and N. Farhat, "The transversal imager: a photonic neurochip with programmable synaptic weights", IEEE Trans. on Neural Networks, vol. 6, pp. 248-251, Jan. 1995.

Copies of these publications are included with this report.
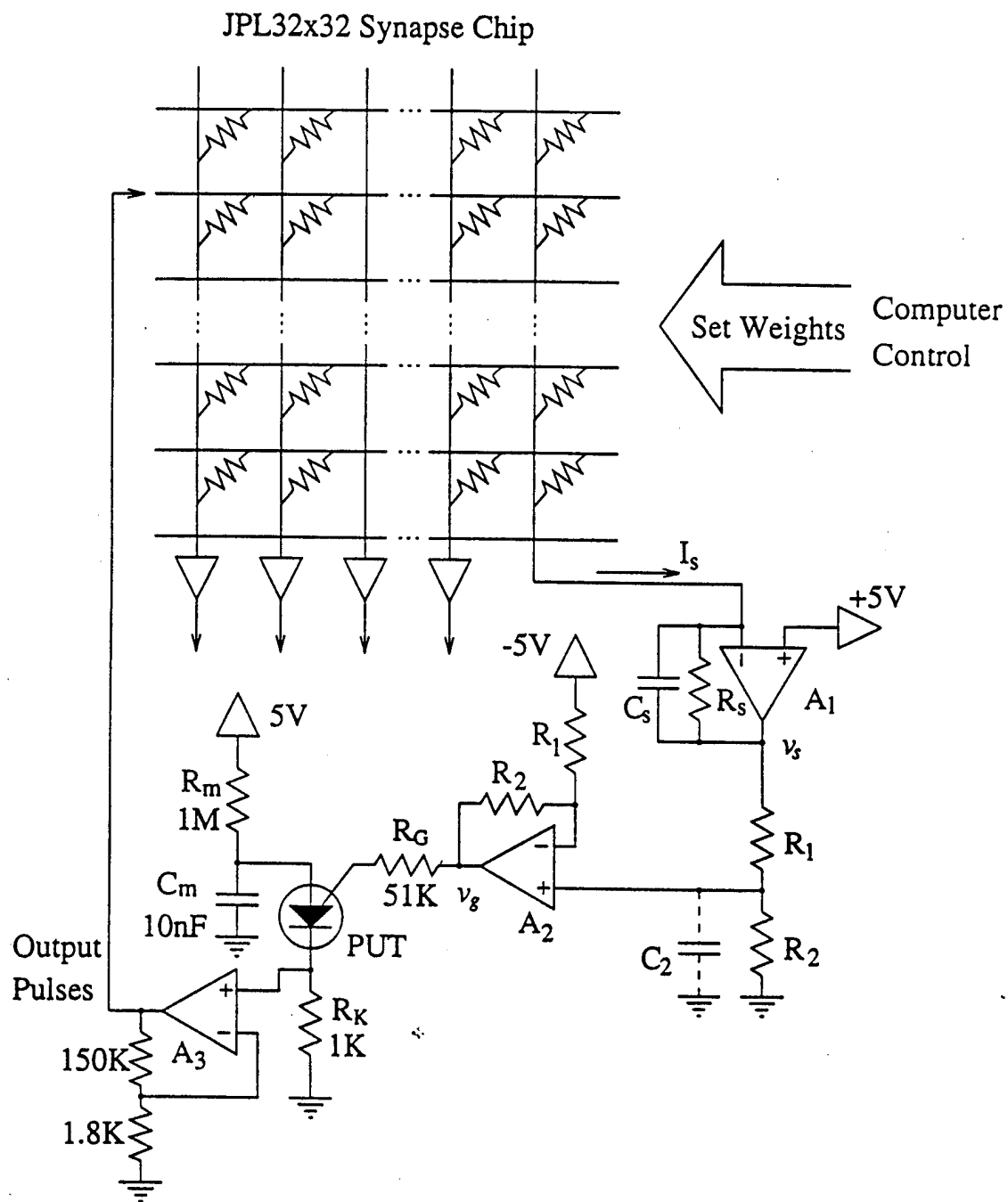
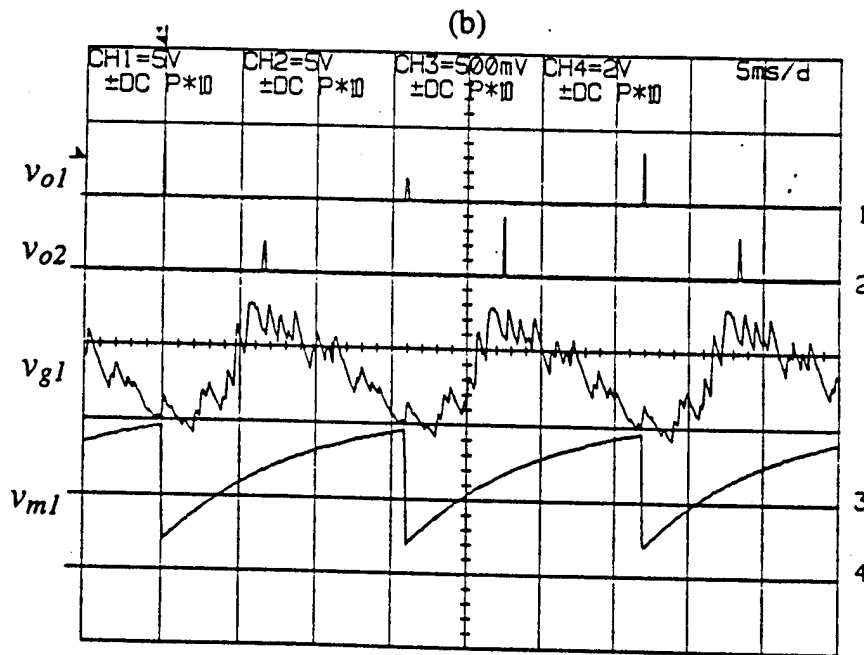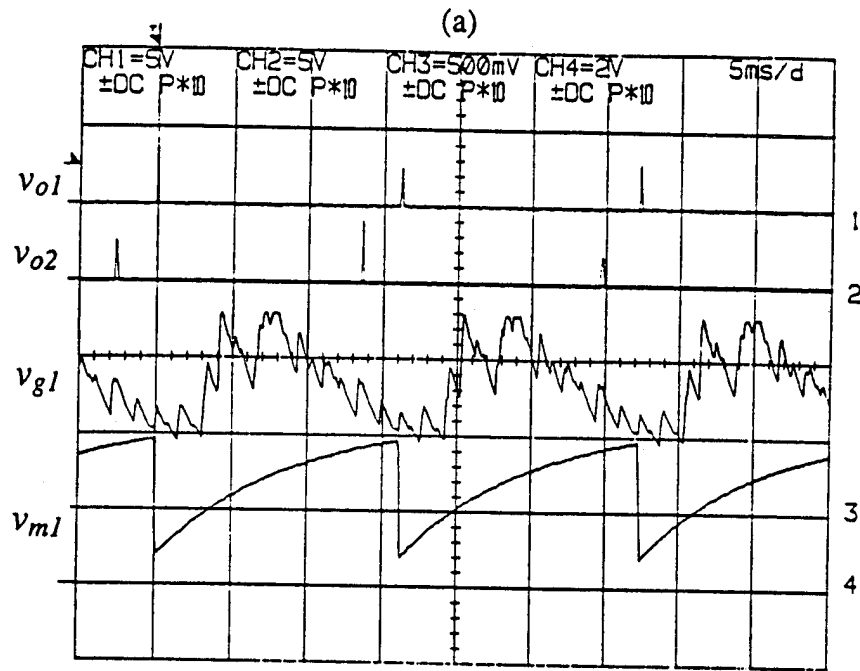Figure 1: Schematic diagram of the network with modulation of the PUTON's threshold voltage.

Figure 2: Two typical waveforms of the network, with symmetric random weights between 0 and −63. Channel 1: output pulses v_{o1} of neuron 1. Channel 2: output pulses v_{o2} of neuron 2. Channel 3: gate voltage v_{g1} of neuron 1. Channel 4: membrane potential v_{m1} of neuron 1.

Optoelectronic neural dendritic tree processing with electron-trapping materials

Z. Wen, A. Baek, and N. H. Farhat

Department of Electrical Engineering, University of Pennsylvania, Philadelphia, Pennsylvania 19104

We show that under simultaneous illumination of pulsed blue light and constant IR light the dynamic responses of electron-trapping materials could be employed to implement optically controlled neural dendritic responses. The importance of neurocomputing with biology-oriented spiking neurons and the role played by dendritic trees are discussed. Computer simulations of dendritic responses in biological neuron and experimental results of electron-trapping material dynamics are presented. These results show that electron-trapping materials are well suited for implementing optically controlled dendritic responses for use in large-scale biology-oriented optoelectronic spiking neural networks.

Electron-trapping materials (ETM's) have received much attention in optical information processing, erasable three-dimensional optical memory, and optical neural networks[1-3] because of their many attractive properties, such as large linear dynamic range, high usable resolution, and fast response times. Recently we initiated a study of the dynamics of ETM's under sumultaneous illumination of blue light and IR light[4] and uncovered a new set of dynamics that makes ETM's uniquely suited for use in optoelectronic implementation of large-scale biology-oriented spiking (or pulsating) neural networks. In a previous Letter we demonstrated the utility of ETM's in producing dense arrays of optoelectronic spiking neurons.[5] In this Letter we describe the use of ETM's in producing optically controlled dendritic responses for optoelectronic spiking neural networks. The importance of neurocomputing with spiking neurons, in particular the role played by the neurons' dendrites, is first discussed. Then computer simulation results of dendritic responses in biological neuron and experimental results of ETM dynamics are presented. It is shown that ETM's are well suited for implementing optically controlled dendritic responses, i.e., postsynaptic responses or potentials, of the kind needed in optoelectronic implementation of large-scale biology-oriented pulsating neural networks.

In contrast to most conventional neural network models studied today, which assume that computational power stems from the massive interconnections (synaptic weights) among the large numbers of functionally simple processing elements (sigmoidal or binary neurons) and which ignore explicitly the spiking nature of biological neurons as well as the role of relative timing between action potentials, biological neurons are both functionally and structurally complex processing elements. It is reasonable to expect that this functional complexity would reflect itself in the higher-level computational power of the networks they form, and therefore development of artificial neuron models that emulate the functional complexity of biological neurons would lead to a new generation of neural networks with vastly enhanced processing power. Recent physiological experimental results strongly support these conjectures (see, e.g., Refs. 6 and 7). The functional complexity of biological neurons stems from two properties: (a) the complex dynamics of the excitable biological membrane and (b) the preprocessing conducted by dendrites on incident spike trains from other neurons. Our study in modeling the excitable biological membrane, based on a limit-cycle oscillator employing an S-shaped nonlinearity that emulates the excitable biological membrane to form what we call bifurcation neuron, shows that the bifurcation neuron model preserves much of the functional complexity of biological neurons and, particularly under periodic activation potential, exhibits complex firing modality such as integer harmonic and subharmonic phase-locked firing, period-m firing, quasi-periodic firing, and period-doubling routes to chaos, depending on the parameters of its periodic activation.[8] A crucial assumption in the above study is that dendritic tree processing produces periodic activation potential when the impinging incident spike trains are coherent. Such coherent incident spike activity occurs whenever a network of spiking neurons phase locks. Therefore dendritic tree processing plays a central role in spiking neural networks in their abilities to phase lock and to exhibit rich functional complexity.

In biological neural networks, the arrival of an action potential at a synapse site on the dendrite of a target neuron triggers a chain of electrochemical events. The result is the production of a postsynaptic potential (PSP) that alters the activation potential (membrane potential) at the target neuron's hillock, which is the trigger zone for action potential generation. The polarity, amplitude, and shape of the PSP waveform depend on the type of neurotransmitter involved in synaptic transmission, on the location of the synapse on the dendritic tree, and on the propagation from the synapse to the hillock. In an actual situation, the activation potential at the hillock of a neuron is the superposition of a large number of such PSP's produced by the barrage of ac-
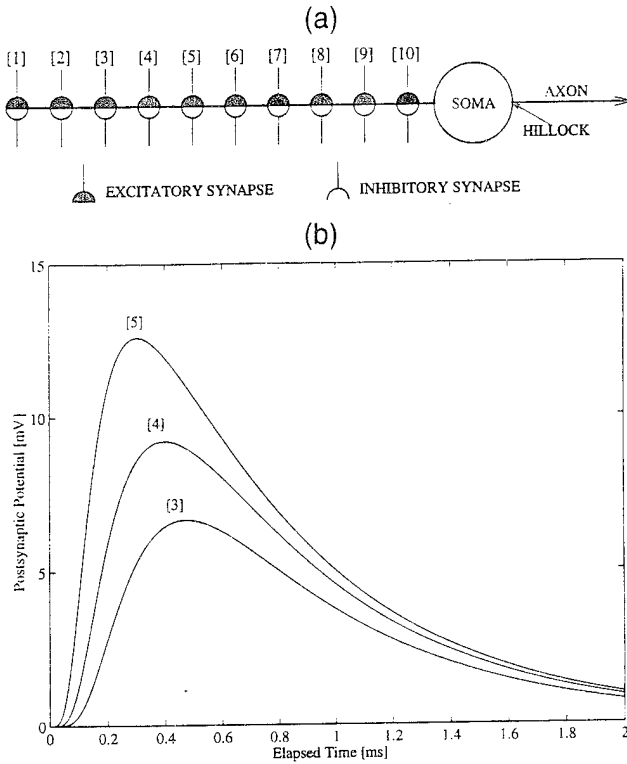
(a)

(b)

Fig. 1. (a) Diagram of a model neuron with a single dendrite with 10 excitatory and 10 inhibitory synapses used in computer simulations of PSP's formed at the hillock by injection of current pulses at selected synapses. (b) PSP's generated by a transient diffusion differential equation of a passive dendrite for three excitatory synapse positions of injected current pulses. Membrane resistance, 50 Ω cm^2; membrane capacitance, 1 μF/cm^2; intracellular resistance, 100 Ω cm (see Ref. 9).

ron's hillock to produce periodic activation potential. Furthermore, such periodic activation is sufficiently robust with fluctuations in synaptic transmission efficacy and, to a lesser extent, in synaptic delay time.

We now show that under simultaneous illumination of pulsed blue light and constant IR light the ETM responses can be used to implement optically controlled dendritic responses. We model ETM dynamics by the following equations[5]:

$$\frac{\mathrm{d}n(t)}{\mathrm{d}t} = \alpha I_B(t) - \beta n(t) I_{\mathrm{IR}}(t), \qquad (1)$$

$$I_O(t) = \kappa I_B(t) + \gamma n(t) I_{\mathrm{IR}}(t), \qquad (2)$$

where $n(t)$ denotes the trapped electron density; $I_B(t)$, $I_{\mathrm{IR}}(t)$, and $I_O(t)$ represent the blue light, the IR light, and the emitted orange light intensities; α and κ are coefficients for trap creation and fluorescence by the blue light; and γ and β are coefficients for IR-stimulated emission and trap erasing by the IR light, respectively. The dynamics of interest here is identical to the situation considered in Ref. 5, i.e., I_{IR} is static and $I_B(t)$ consists of a static term and a pulse-modulated term as follows:

$$I_B(t) = I_0 + I_1 \sum_{k=0}^{k=\infty} [u(t - kT) - u(t - kT - t_w)], \quad (3)$$

where $u(t)$ denotes the unit step function, I_0 and I_1 are the static and pulsed blue light intensities, and T and t_w are the pulse period and the pulse width, respectively. The solution for the emitted orange light $I_O(t)$ during the Nth period is[5]

$$I_O(t) = \begin{cases} \kappa(I_0 + I_1) + \dfrac{\alpha\gamma I_0}{\beta} + \alpha\gamma I_1 I_{\mathrm{IR}} \left\{ \dfrac{t_w}{[\exp(\beta I_{\mathrm{IR}} T) - 1]} + t - NT \right\} & \text{for } NT < t < NT + t_w \\[3ex] \kappa I_0 + \dfrac{\alpha\gamma I_0}{\beta} + \alpha\gamma I_1 I_{\mathrm{IR}} t_w \dfrac{\exp[-\beta I_{\mathrm{IR}}(t - NT - t_w)]}{[1 - \exp(-\beta I_{\mathrm{IR}} T)]} & \text{for } NT + t_w < t < (N+1)T \end{cases} \qquad (4)$$

tion potentials from other neurons arriving at any time at the synapse sites on its dendrites. The importance of dendritic tree processing was studied recently.[9,10] By assuming the dendrite to be passive, it is possible for one to derive a transient diffusion differential equation (the cable equation) and to determine the response of a dendrite to current pulses injected at different positions along its length.[9] Injected current pulses represent the effect of arriving action potentials. Using commonly listed dendritic parameters,[9] we have carried out such a computation for the simplified arrangement shown in Fig. 1(a) for current pulses of uniform amplitude injected at three synapses along the dendrite. The results, given in Fig. 1(b), show how the shape of the PSP and its rise time, peak value, latency (peak position), and decay time all depend on synapse position (i.e., position of injected current). In reality, the peak value also depends on the synaptic efficacy. We also carried out simulations that confirm that when the incident spike trains are correlated, the smoothing responses of dendrites lead to PSP's that sum at the neu-

From Eq. (4) we observe that in the emitted orange light the contributions that are due to IR-stimulated emission and fluorescence coexist. Fluorescence is manifested by sudden jumps at the onset and termination of the blue light pulses. On the other hand, IR-stimulated emission first undergoes a linear increase during the blue light pulse in the charging process and then decays exponentially after the pulse in the discharging process. An experiment has been carried out to study ETM dynamics in the above situation by using the same experimental setup used in Ref. 5. Figure 2 shows the experimental results. In all these plots, $I_1 = 3.98$ mW/cm^2, $t_w = 25$ ms, and $T = 250$ ms. Figure 2(a) shows the ETM responses for three different levels of the static blue light intensity I_0, whereas the IR light intensity I_{IR} is constant. In Figs. 2(b) and 2(c), I_0 remains unchanged, whereas I_{IR} is varied. From Fig. 2 one observes the fluorescence jumps at the blue light pulse edges, linear buildup during the pulse, and trailing exponential decay after it, as predicted by Eq. (4). Equation (4) indicates that varying I_0 shifts the ETM response up
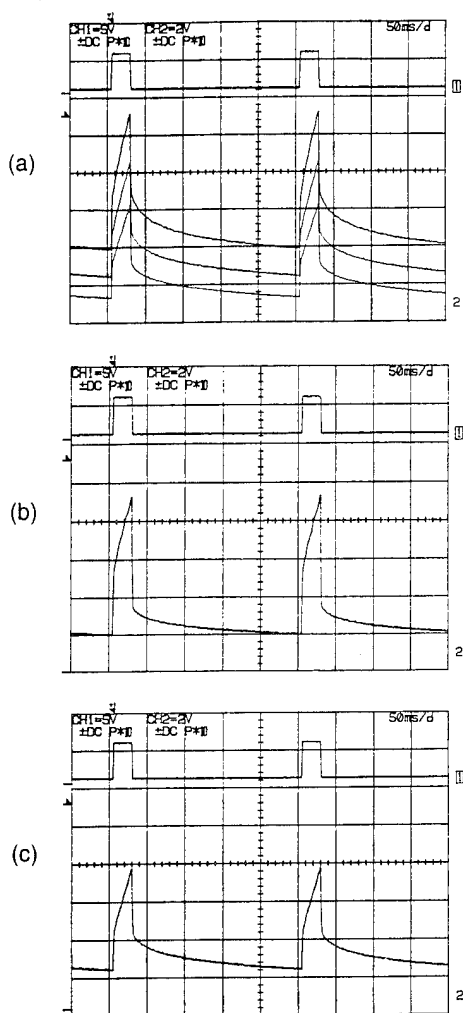
Fig. 2. Oscilloscope displays of ETM responses. Upper trace: Pulsing signal from the programmable liquid-crystal beam gate (see Fig. 1 of Ref. 5). Lower trace: ETM responses. (a) $I_{IR} = 403$ mW/cm^2, $I_0 = 4.8$ μW/cm^2 (lower curve), 0.22 mW/cm^2 (middle curve), and 0.54 mW/cm^2 (upper curve). (b) $I_{IR} = 128$ mW/cm^2, $I_0 = 29.4$ μW/cm^2. (c) $I_{IR} = 372$ mW/cm^2, $I_0 = 29.4$ μW/cm^2.

and down, and the results shown in Fig. 2(a) generally agree with this. The results in Fig. 2 show, however, that the heights of the fluorescence jumps, as well as the magnitude of the exponential portion of ETM response, vary with I_{IR} and I_0 used. Furthermore, it appears that the upward jump and the downward jump have different heights. The first-order linear model of ETM dynamics given in Eqs. (1) and (2) fails to predict these subtle effects because it neglects nonlinear effects such as trapped electron density saturation and dependence of electron-trapping efficiency on existing trapped electron density. Clearly, to utilize ETM's effectively in applications that make use of their unique dynamics it is necessary to develop an improved theoretical model that would take into account the neglected effects mentioned above. We are in the process of developing such a model and verifying it experimentally; the results will be reported elsewhere. Nonetheless, we draw attention now to the similarity between the PSP's in Fig. 1, which represent bio-

logical neurons, and the ETM responses in Fig. 2. By varying the values of I_0 and/or I_{IR}, one can control the ETM response in various ways, e.g., up and down shifts, different heights of fluorescence jumps and magnitude of exponential response, and faster or slower exponential decays. So we have a unique method for crudely emulating dendritic response in biological neurons in a fashion useful for realizing a dense optically controlled dendritic response array (or two-dimensional dendritic trees) for use in large-scale biology-oriented optoelectronic spiking neural networks.

The spiking nature of biology-oriented neural networks makes studying their behavior by computer simulation impractical because of the lengthy computing time involved. In a recent paper Prange and Klar.[11] argued convincingly that the best way of studying and realizing biology-oriented neural networks is through analog complementary metal-oxide semiconductor technology rather than digital hardware. However, they showed that the number of neurons one can accommodate on a VSLI chip is limited to a hundred or so, even when submicrometer complementary metal-oxide semiconductor technology is used, because of the relatively large size of the neuron/dendrite cell. By combining ETM's with state-of-the art technologies such as smart pixel spatial light modulators and image intensifiers to form dense arrays of spiking neurons and dendritic responses, it is feasible that large-scale optoelectronic spiking neural networks of $10^3 - 10^4$ neurons can be realized. Such networks would be invaluable tools for modeling, studying, and demonstrating the role of synchronicity, bifurcation, and chaos in higher-level cortical functions and exploring their use in enhancing the performance of artificial neural systems.

References

1. S. Jutamulia, G. M. Storti, J. Lindmayer, and W. Seiderman, Appl. Opt. **30,** 2879 (1991).
2. X. Yang, C. Y. Wrigley, and J. Lindmayer, Proc. Soc. Photo-Opt. Instrum. Eng. **1773,** 413 (1992).
3. A. D. McAulay, J. Wang, and X. Xu, Appl. Opt. **32,** 1346 (1993).
4. Z. Wen, N. H. Farhat, and Z. J. Zhao, Appl. Opt. **32,** 7251 (1993).
5. Z. Wen, N. H. Farhat, and S. Y. Lin, Opt. Lett. **19,** 1394 (1993).
6. C. M. Gray and W. Singer, Proc. Natl. Acad. Sci. USA **86,** 1698 (1989).
7. R. Eckhorn, H. J. Reitboeck, M. Arndt, and P. Dicke, Neural Comput. **2,** 293 (1990).
8. N. H. Farhat, S. Y. Lin, and M. Eldefrawy, Proc. Soc. Photo-Opt. Instrum. Eng. **CR55,** 77 (1994).
9. T. McKenna, J. Davis, and S. F. Zornetzer, *Single Neuron Computation* (Academic, San Diego, Calif., 1992).
10. J. G. Elias, Neural Comput. **5,** 648 (1993).
11. S. Prange and H. Klar, in *Neurobionics*, W. Both, M. Sami, and R. Eckmiller, eds. (Elsevier, Amsterdam, 1993), p. 225.

Brief Papers

The Transversal Imager: A Photonic Neurochip with Programmable Synaptic Weights

J. R. Tower and N. Farhat

Abstract— A photonic neural processor implemented in NMOS/CCD integrated circuit technology is described. The processor performs outer-product processing utilizing optical input of the synaptic weights and electrical input of the state vector, or, visa versa. The performance of the 32-neuron, 1024-synapse processor is presented.

I. INTRODUCTION

THIS paper describes the design, fabrication, and performance of an NMOS/CCD integrated circuit which performs outer-product, neural network computations. The transversal imager integrated circuit utilizes a unique architecture which permits (1) the synaptic weights to be introduced electrically to the complete neural network in parallel, and the one-dimensional state vector to be introduced optically, or (2) the synaptic weights to be introduced optically to the complete neural network in parallel, and the one dimensional state vector to be introduced electrically. In both cases, the computation of the outer-product between the two-dimensional synaptic weight matrix and the one-dimensional state vector is performed simultaneously across the integrated circuit.

The optical input to this electro-optical neural network can thus be reduced to the one-dimensional state vector. This simplification of the optical input requirements from a two-dimensional pattern to a one dimensional pattern has significant impact on system hardware performance, and system computational throughput.

II. DESCRIPTION OF PROCESSING ALGORITHM

As background for understanding the transversal imager architecture, it is useful to discuss the motivation for the architecture, namely, the efficient implementation of the Hopfield neural network. In the basic Hopfield neural network [1], there are N neurons which are connected to each other by the synapses. The state of the network is given by the vector V:

$$V = (V_1, V_2, \cdots V_N).$$

The network interconnections are designated by the synaptic interaction matrix W, whereby the weight W_{ij} is the strength of the interaction from the jth neuron to the ith neuron. The

synaptic matrix is of dimension $N \times N$. The state of network is updated according to (1) the vector-matrix multiplication:

$$I_i = \sum W_{ij} V_j$$

and (2) a transfer function:

$$V_i = f(I_i)$$

where V_i is the updated state of the ith neuron. The state of the neuron is either excited ($V_i = 1$) or not excited ($V_i = 0$). The interconnection weights are either unipolar binary [$W_{ij}\varepsilon 0$(off), $+1$(excite)], bipolar binary [$W_{ij}\varepsilon - 1$ (inhibit), $+1$(excite)], ternary [$W_{ij}\varepsilon - 1$ (inhibit), 0 (off), $+1$ (excite)], or analog. The transfer function is typically a sharp thresholding function.

III. PRIOR CCD NEURAL NETWORK APPROACHES

All of the charge coupled device neural processing integrated circuits reported to date (1) exploit the analog, rather than digital, capability of CCD's, and (2) use charge domain processing to reduce the area required for interconnections and computational circuitry. In the work reported by Sage *et al.* of MIT Lincoln Laboratories [2], surface channel CCD technology and metal nitride oxide semiconductor (MNOS) technology is combined to produce circuits capable of outer product processing. In this approach, state vectors are introduced electrically, and the analog synaptic weights are produced electrically and stored in MNOS gates. The MNOS-CCD gates function to store the synaptic weight and to control the flow of charge, thereby producing the product of the input state and the stored weight. The sum of products is produced in the charge domain and then converted to the voltage domain to produce, in a Hopfield net application, the desired outer-product result.

In the CCD neural network processor work by Chiang *et al.* of MIT Lincoln Laboratory [3], buried channel CCD structures are utilized for a variety of functions including the implementation of multiplying digital-to-analog converters (MDAC's). In this architecture, when applied to the Hopfield algorithm, the state vector is introduced electrically to an analog CCD register. The synaptic weights are introduced electrically to 6-bit CCD digital memories. The MDAC's perform the outer-product multiplication of the analog state vector and the 6-bit digital synaptic weights, with the summation of products being achieved in the charge domain. The output charge packets are

Fig. 1.   Transversal imager architecture.

(a)

(b)

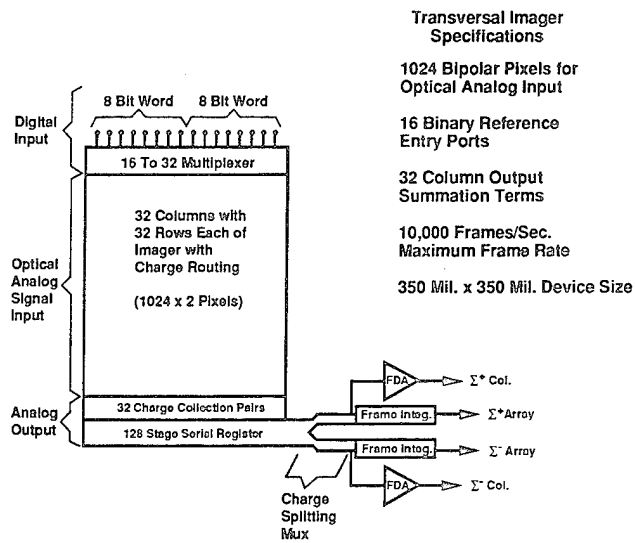Fig. 2.   (a) Transversal imager configured for optical input of state vector. (b) Transversal imager configured for optical input of synaptic weights.

then converted into the voltage domain to produce the final outer product result.

The CCD neural processor which is most similar to the transversal imager is that reported by Agranat, *et al.* of the California Institute of Technology [4]. In this work a Hopfield network is realized utilizing buried channel CCD technology. The state vector input is binary $(+1, 0)$ and is introduced electrically. The synaptic weights are input electrically or optically, and are analog. The outer product multiplication of the binary state vector and each analog synaptic weight is performed by controlled $(+1$ charge flow, 0 no charge flow) gating of replicas of the recirculating synaptic weights. The gated products are added together in the charge domain, forming the outer product sum-of-products. The outer product terms are then serially read out in the charge domain to an output where the final voltage output is produced. This architecture therefore utilizes a two-dimensional optical input to introduce the analog synaptic weights, and the binary state vector is introduced electrically.

IV. TRANSVERSAL IMAGER ARCHITECTURE

The transversal imager concept grew out of work conducted in the late-1970's and early 1980's in the field of programmable CCD analog-binary transversal filters [5], [6]. The transversal imager architecture we use is shown in Fig. 1. This signal processing imager [7], [8] was designed to perform vector-matrix multiplication by (1) imaging the one-dimensional input state vector (V) spread across the rows of the $N \times N$ image area, (2) performing the interconnect, synaptic weighting (W) at each pixel location in parallel, (3) performing the summation along each column in parallel, and (4) reading out the sum-of-products terms serially. The architecture was chosen to realize the following desirable features:

1) Optical input of the one-dimensional state vector.
2) Electrical input of the matrix weighting at each vector-matrix multiplication.
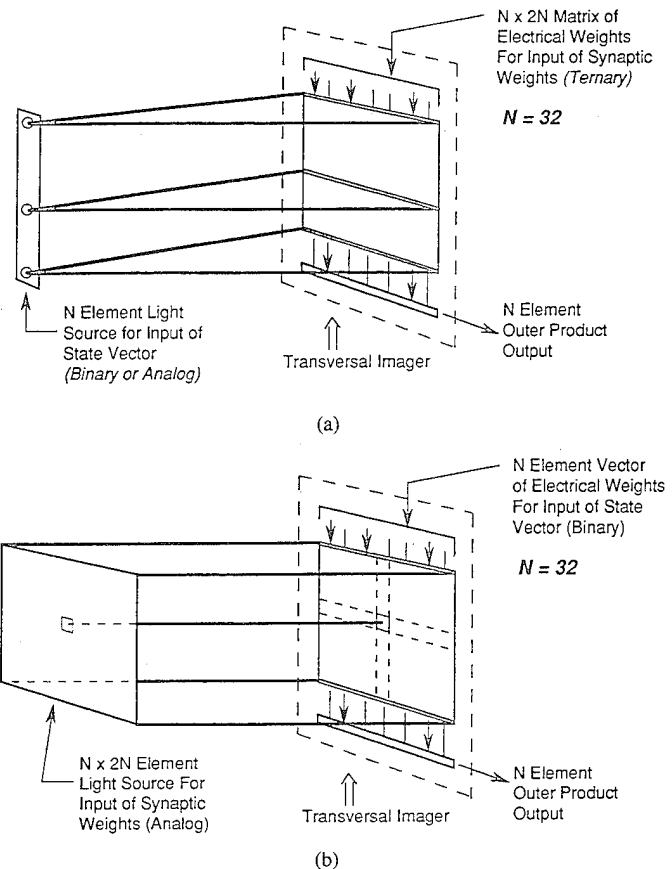
3) Simultaneous ternary weighting $(-1, 0, +1)$ at each pixel.
4) High vector-matrix multiplication frame rate; with frame rate dominated by serial output register readout rate.
5) High optical integration time duty-cycle; with integration time a very high percentage of frame rate.

Each pixel of the transversal imager consists of two photo-capacitors which see the same optical input, two stages of an NMOS digital shift register, control gates, and summation busses $(\sum^+ \text{ and } \sum^-)$. The ternary weighting is achieved by controlling the transfer of the photocharge integrated in the two photo-capacitors. If both photo-capacitors contribute charge to the summation plus $(\sum^+)$ bus the pixel weight is $+1$, if both contribute to the summation minus $(\sum^-)$ bus the pixel weight is -1, and if one contributes to the $\sum^+$ while the other contributes to the $\sum^-$, the weight is 0.

The NMOS digital shift registers control the selective transfer of photocharge to the $\sum^+$ bus based on the data in the shift register. Once the selective transfer to the column $\sum^+$ busses is completed, all of the photo-capacitors transfer the remaining charge to the respective column $\sum^-$ busses. In this fashion the imaged photocharge is weighted in parallel by selective charge transfer.

The column $\sum^+$ and $\sum^-$ busses receive the photocharge and perform a nearly instantaneous summation of the column products in the charge domain. The weighted and summed photocharge from the N columns are pulled off of the $N - \sum^+$

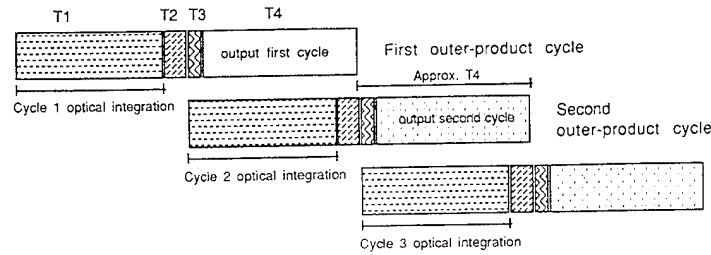Fig. 3. Transversal imager operating cycle.

and $N-\sum^{-}$ busses and transferred into a serial output register by charge primed couplers [9]. The serial output register switches the $\sum^{+}$ and $\sum^{-}$ signals to respective floating diffusion output amplifiers after appropriate stage delays. The $\sum^{+}$ and $\sum^{-}$ output amplifiers are differentially sensed to produce the desired outer product result.

The primary operating configuration is shown schematically in Fig. 2(a). The optical input of the state vector is provided by a display, or more commonly an N element LED array and anamorphic optics, which spreads the light across the rows of the transversal imager. The state vector may be analog, but is usually confined to a binary on or off. Each of the N (LED) elements illuminates all of the photo-capacitor pairs in it's associated row. The $N \times 2N$ elements of the ternary synaptic weight matrix are introduced through multiple parallel electrical input ports.

An alternate operating configuration is shown schematically in Fig. 2(b). In this configuration, the synaptic weights are input optically. A display with $N \times 2N$ resolution elements or a spatial light modulator with at least $N \times 2N$ elements projects the weights. The state vector is introduced electrically with either unipolar binary, bipolar binary, or ternary weights. The power of this approach is that bipolar analog synaptic weights may be achieved with this configuration. Thus, a continuous range of both inhibitory and excitatory weights may be introduced to the outer product.

V. OPERATING CYCLE

To maximize the speed of the transversal imager the device was designed to perform simultaneous operations. The device operating cycle starts with the initiation of the electrical weight read-in through multiple digital input ports ($T1$). At the completion of the operation, the weighting and summation is performed by selective transfer of the photocharge ($T2$). The sum-of-product terms are then transferred into the serial output register ($T3$). This is followed by serial readout and development of the final outer-product terms ($T4$).

The optical input and the integration of the photocharge may occur continually. The only time period where erroneous signal can be produced is during the selective transfer (weighting) process. This time period is a very small portion of the complete cycle time. Therefore, a choice can be made between either a small error in the signal with the optical input always present or an operational procedure whereby the optical input is turned off during the selective transfer process.

The high optical duty cycle and the rapid weighting operation are complemented by a design which permits a rapid

transfer into the serial output register. These characteristics contribute to a high sensitivity and a total latency which is dominated by the serial output rate.

To assure that the weight introduction process is not adversely impacting the transversal imager cycle time, the digital register design incorporates multiple input ports and a digital clock rate such that the weight introduction time ($T1$) is less than the serial readout time ($T4$). Furthermore, the weighting/summation process ($T2$) and the transfer into the serial register ($T3$) are rapid compared to the serial readout time ($T4$). Thus, the device may be run in the manner shown in Fig. 3, assuring a cycle time essentially equal to the serial output register readout time ($T4$).

An approximation of analog synaptic weights can be achieved with this processor architecture. By performing the above described operating cycle on a series of synaptic weight "bit planes," accumulating the outer product terms, and then applying the appropriate $1/2^{n}$ weighting, the synaptic weights can be implemented to n-bits. The penalty of this increased resolution in the weights is the increase from a single computational cycle to n cycles.

VI. PERFORMANCE RESULTS

A 32×32 transversal imager has been fabricated in a 3-μm NMOS/ buried channel CCD process. The device has a square 200×200-μm pixel pitch. (The pixel size is primarily determined by coarse metal design rules, since the host device on the wafer is a back-side illuminated, thinned visible imager.) Each pixel consists of two photo-capacitors, two stages of digital shift register, and the associated circuitry to perform ternary weighting.

The results shown are for a serial output register rate of 1.0 MHz. The various $T1$, $T2$, $T3$, $T4$ portions of the cycle are being run non-overlapped to simplify the operating electronics requirements. The resulting cycle rate is 2500 cycles/s. In this operating mode, 8×10^{4} differentially sensed outer-product terms are produced per second.

One of the advantages of the transversal imager architecture is that the operating cycle does not change if the operating mode is changed. The same operating cycle is utilized in the optical state vector and electrical synaptic weights mode as is used in the optical synaptic weights and electrical state vector mode. The transversal imager therefore sustains the same outer-product rate in either mode.

In the results presented below, the actual photocharge weighting and summation in the charge domain is completed in parallel across the complete array in a time $T2 = 20$ μs.
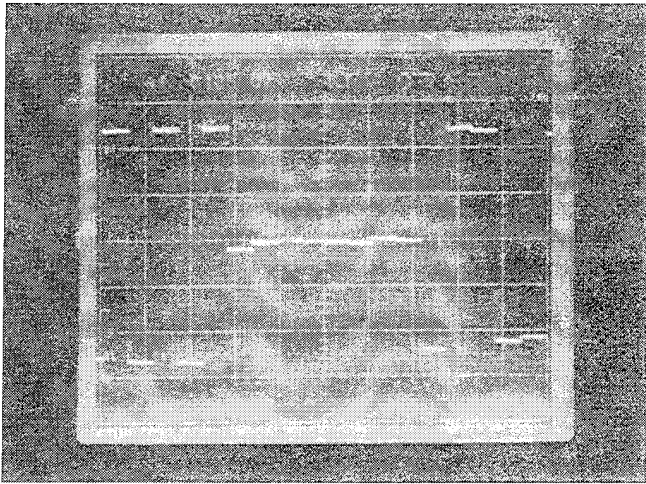
Fig. 4. Final outer-product result for uniform optical vector input and ternary synaptic weights.
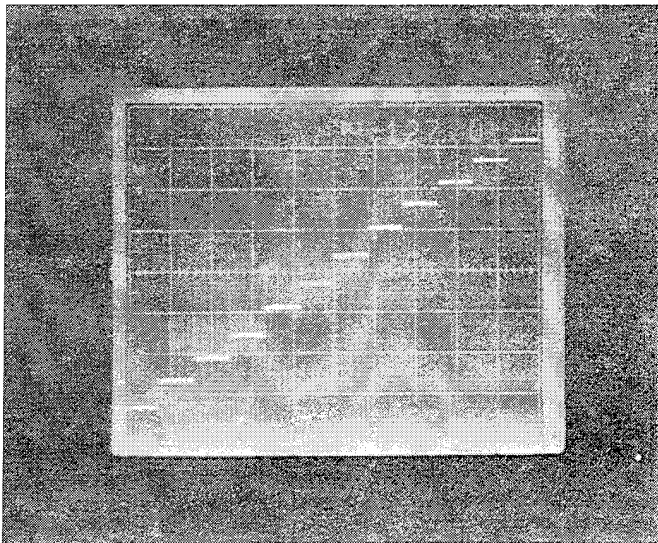

Fig. 5. Final outer-product result for linearly increasing optical vector input and uniform negative synaptic weights.

This time is dominated by the photocharge thermal diffusion transfer time, which is long given the large pixels. In this 20 μs period 2000 analog-binary multiplications and 2000 additions are performed.

The preliminary results shown in Fig. 4 show the final differential output of 18 columns for a uniform light input and a complete column weighting of (left-to-right): $+ - + -$ $+0000\ 0000 - + + - -$. (A portion of the small non-uniformity in response is due to non-uniform illumination.) Fig. 5 shows the final transversal imager output for a uniform negative weight and a wedge-shape optical input pattern.

VII. CONCLUSION

A novel electro-optical neural network processor has been developed. The processor is based on MOS/CCD integrated circuit technology. The 32 × 32 transversal imager demonstrated performs ternary weighting. This first implementation

utilizing a 200 × 200-μm cell pitch, 1.5-MHz clocking, and a non-overlapping operating cycle achieves 5 000 000 analog binary operations/s (2 500 000 multiplications, and 2 500 000 additions). As a neural network processor the current implementation achieves 32 fully interconnected neurons with an interconnection update rate of 2.5×10^6 interconnection updates/s.

This architecture, the overlapped operating cycle discussed, and today's silicon IC technology would permit scaling to a 75 × 75-μm cell pitch and 10-MHz clocking. This would permit realization of a 128 × 128 processor with 128 fully interconnected neurons processing at an update rate of 7×10^8 interconnection updates per second. Furthermore, the architecture permits, even at these high processing rates, the optical input and the electrical input to both be updated during each cycle. This would be very useful for learning algorithms where it is desirable to update the synaptic weights frequently.

The architecture permits extension to larger neural networks by tiling of the transversal imager devices in 2 × 2 or 4 × 4 mosaics. In the configuration with optical input of the state vector, to achieve these larger networks, an optical input device with twice or four times the number of elements would be required. The optical input would be spread across the rows of the mosaic and the column partial outer-product outputs from each device would be combined within the columns of the mosaic to produce the desired outer-product result. The transversal imager devices would be run in parallel with common clocking signals. In this manner the architecture can be extended to realization of larger electro-optical neural processors.

REFERENCES

[1] J. J. Hopfield, "Neural networks and physical systems with emergent collective computational abilities," *Proc. Nat. Acad. Sci.*, vol. 79, pp. 2554–2558, 1982.
[2] J. P. Sage, K. Thompson, and R. S. Withers, "An artificial neural network integrated circuit based on MNOS/CCD principles," in *Appl. Inst. Phy. Conf. Proc.*, 1986.
[3] A. Chiang, R. Mountain, J. Reinold, J. LaFranchise, and G. Lincoln, "A programmable CCD signal processor," in *IEEE Int. Solid-State Circ. Conf.*, 1990, pp. 146–148.
[4] A. J. Agranat, C. F. Neugebauer, R. D. Nelson, and A. Yariv, "The CCD neural processor: A neural network integrated circuit with 65 536 programmable analog synapses," *IEEE Trans. Circ. Syst.*, vol. 37, pp. 1073–1075, Aug. 1990.
[5] D. A. Gandolfo, J. R. Tower, J. I. Pridgen, and S. C. Munroe "Analog-binary CCD correlator: A VLSI signal processor," *IEEE Trans. Electron Dev.*, vol. ED-26, pp. 596–603, Apr. 1979.
[6] J. R. Tower, R. L. Angle, D. S. Kent, L. E. Elliott, D. A. Gandolfo, and R. F. Sproat, "A CMOS/CCD 256 stage programmable transversal filter," *IEEE J. Solid-State Circ.*, vol. SC-17, pp. 1062&n dash;1069, Dec. 1982.
[7] J. R. Tower, U. S. Patent 4,514,821, Apr. 30, 1985.
[8] J. R. Tower, "Development of electro-optical neural network signal processing techniques employing custom charge coupled devices," Ph. D. dissertation proposal, Univ. of Pennsylvania, Philadelphia, PA, May 1986.
[9] K. Senda, S. Terakawa, Y. Hiroshima, and T. Kunii, "Analysis of charge priming transfer efficiency in CPD image sensors," *IEEE Trans. Electron Dev.*, vol. ED-31, pp. 1324–1328, Sept. 1984 .

REPORT DOCUMENTATION PAGE

Form Approved
OMB No. 0704-0188

Public reporting burden for this collection of information is estimated to average 1 hour per response, including the time for reviewing instructions, searching existing data sources, gathering and maintaining the data needed, and completing and reviewing the collection of information. Send comments regarding this burden estimate or any other aspect of this collection of information, including suggestions for reducing this burden to Washington Headquarters Services, Directorate for Information Operations and Reports, 1215 Jefferson Davis Highway, Suite 1204, Arlington, VA 22202-4302, and to the Office of Management and Budget, Paperwork Reduction Project (0704-0188), Washington, DC 20503.

1. AGENCY USE ONLY (Leave blank)	2. REPORT DATE 04/01/95	3. REPORT TYPE AND DATES COVERED Quarterly - 01/01/95 - 04/01/95

4. TITLE AND SUBTITLE	5. FUNDING NUMBERS
COGNITIVE NETWORKS FOR ATR: THE ROLES OF BIFURCATION AND CHAOS	N00014-94-1-0931

6. AUTHOR(S)

N.H. Farhat

7. PERFORMING ORGANIZATION NAME(S) AND ADDRESS(ES)	8. PERFORMING ORGANIZATION REPORT NUMBER
N.H. Farhat University of Pennsylvania Electrical Engineering Department 200 South 33rd Street Philadelphia, PA 19104-6390	3rd Quarterly Report

9. SPONSORING/MONITORING AGENCY NAME(S) AND ADDRESS(ES)	10. SPONSORING/MONITORING AGENCY REPORT NUMBER
Scientific Officer Code: 4414 William Miceli - Office of Naval Research Ballston Tower One 800 North Quincy Street Arlington, VA 22217-5660	

11. SUPPLEMENTARY NOTES

12a. DISTRIBUTION/AVAILABILITY STATEMENT	12b. DISTRIBUTION CODE

13. ABSTRACT (Maximum 200 words)

Quarterly Report (No Abstract)

14. SUBJECT TERMS		15. NUMBER OF PAGES 12
		16. PRICE CODE

17. SECURITY CLASSIFICATION OF REPORT	18. SECURITY CLASSIFICATION OF THIS PAGE	19. SECURITY CLASSIFICATION OF ABSTRACT	20. LIMITATION OF ABSTRACT
UNCLASSIFIED	UNCLASSIFIED	UNCLASSIFIED	

NSN 7540-01-280-5500

OFFICE OF THE UNDER SECRETARY OF DEFENSE (ACQUISITION)
DEFENSE TECHNICAL INFORMATION CENTER
CAMERON STATION
ALEXANDRIA, VIRGINIA 22304-6145

SUBJECT: Distribution Statements on Technical Documents

TO: OFFICE OF NAVAL RESEARCH
     CORPORATE PROGRAMS DIVISION
     ONR 353
     800 NORTH QUINCY STREET
     ARLINGTON, VA 22217-5660

1. Reference: DoD Directive 5230.24, Distribution Statements on Technical Documents, 18 Mar 87.

2. The Defense Technical Information Center received the enclosed report (referenced below) which is not marked in accordance with the above reference.

REPORT
N00014-94-1-0931
TITLE: COGNITIVE NETWORKS FOR
ATR: THE ROLES OF BIFURCATION AND
CHAOS

3. We request the appropriate distribution statement be assigned and the report returned to DTIC within 5 working days.

4. Approved distribution statements are listed on the reverse of this letter. If you have any questions regarding these statements, call DTIC's Cataloging Branch, (703) 274-6837.

FOR THE ADMINISTRATOR:

1 Encl

GOPALAKRISHNAN NAIR
Chief, Cataloging Branch

FL-171
Jul 93

DISTRIBUTION STATEMENT A:

APPROVED FOR PUBLIC RELEASE: DISTRIBUTION IS UNLIMITED

DISTRIBUTION STATEMENT B:

DISTRIBUTION AUTHORIZED TO U.S. GOVERNMENT AGENCIES ONLY;
(Indicate Reason and Date Below). OTHER REQUESTS FOR THIS DOCUMENT SHALL BE REFERRED
TO (Indicate Controlling DoD Office Below).

DISTRIBUTION STATEMENT C:

DISTRIBUTION AUTHORIZED TO U.S. GOVERNMENT AGENCIES AND THEIR CONTRACTORS;
(Indicate Reason and Date Below). OTHER REQUESTS FOR THIS DOCUMENT SHALL BE REFERRED
TO (Indicate Controlling DoD Office Below).

DISTRIBUTION STATEMENT D:

DISTRIBUTION AUTHORIZED TO DOD AND U.S. DOD CONTRACTORS ONLY; (Indicate Reason
and Date Below). OTHER REQUESTS SHALL BE REFERRED TO (Indicate Controlling DoD Office Below).

DISTRIBUTION STATEMENT E:

DISTRIBUTION AUTHORIZED TO DOD COMPONENTS ONLY; (Indicate Reason and Date Below).
OTHER REQUESTS SHALL BE REFERRED TO (Indicate Controlling DoD Office Below).

DISTRIBUTION STATEMENT F:

FURTHER DISSEMINATION ONLY AS DIRECTED BY (Indicate Controlling DoD Office and Date
Below) or HIGHER DOD AUTHORITY.

DISTRIBUTION STATEMENT X:

DISTRIBUTION AUTHORIZED TO U.S. GOVERNMENT AGENCIES AND PRIVATE INDIVIDUALS
OR ENTERPRISES ELIGIBLE TO OBTAIN EXPORT-CONTROLLED TECHNICAL DATA IN ACCORDANCE
WITH DOD DIRECTIVE 5230.25, WITHHOLDING OF UNCLASSIFIED TECHNICAL DATA FROM PUBLIC
DISCLOSURE, 6 Nov 1984 (Indicate date of determination). CONTROLLING DOD OFFICE IS (Indicate
Controlling DoD Office).

The cited documents has been reviewed by competent authority and the following distribution statement is
hereby authorized.

_____   OFFICE OF NAVAL RESEARCH   _____
(Statement)   CORPORATE PROGRAMS DIVISION   (Controlling DoD Office Name)
                                 ONR 353
                                 800 NORTH QUINCY STREET
                                 ARLINGTON, VA 22217-5660

_____   _____
(Reason)   (Controlling DoD Office Address,
                                                                             City, State, Zip)
                         DEBRA T. HUGHES
                         DEPUTY DIRECTOR
                         CORPORATE PROGRAMS OFFICE
_____   _____   _____
(Signature & Typed Name)   (Assigning Office)   (Date Statement Assigned)